DI-MISC-80048/M Scientific and Technial Reports Summary (Cont'd)
Block 10 PREPARATION INSTRUCTIONS (Con'd)

(2)

AD-A259 066

DOCUMENTATION PAGE

Form Approved OMB No. 0704-01

DTIC ELECTE S DEC 08 1992 A D

1a. REPORT SECURITY CLASSIFICATION: UNCLASSIFIED	1b. RESTRICTIVE MARKINGS: NONE
2a. SECURITY CLASSIFICATION AUTHORITY: N/A	3. DISTRIBUTION/AVAILABILITY OF REPORT: APPROVED FOR PUBLIC RELEASE: DISTRIBUTION IS UNLIMITED N/A
2b. DECLASSIFICATION/DOWNGRADING SCHEDULE: N/A	
4. PERFORMING ORGANIZATION REPORT NUMBER(S): FINAL REPORT	5. MONITORING ORGANIZATION REPORT NUMBER(S): N/A
6a. NAME OF PERFORMING ORGANIZATION: XONTECH INC.	6b. OFFICE SYMBOL (If applicable): N/A
6c. ADDRESS (City, State, and ZIP Code): 1 Pacific Plaza, 7711 Center Ave Suite 550, Huntington Beach, CA 92647	7a. NAME OF MONITORING ORGANIZATION: N/A
8a. NAME OF FUNDING/SPONSORING ORGANIZATION: U. S. Army Strategic Defense Command	8b. OFFICE SYMBOL (If applicable): W31RPD
8c. ADDRESS (City, State, and ZIP Code): P.O. Box 1500, Huntsville, AL 35807-3801	7b. ADDRESS (City, State, and ZIP Code): N/A
	9. PROCUREMENT INSTRUMENT IDENTIFICATION NUMBER: N/A
	10. SOURCE OF FUNDING NUMBERS: PROGRAM ELEMENT NO. / PROJECT NO. / TASK NO. / WORK UNIT ACCESSION

11. TITLE (Include Security Classification): Tracking Radar Advanced Signal Processing and Computing for Kwajalein ATOLL (KA) Application (Unclassified)

12. PERSONAL AUTHOR(S): Cottrill, Stanley D.

13a. TYPE OF REPORT	13b. TIME COVERED	14. DATE OF REPORT (Year, Month, Day)	15. PAGE COUNT
Final	FROM 12/16/91 TO 11/16/92	11/9/92	42

16. SUPPLEMENTARY NOTATION: N/A

17. COSATI CODES			18. SUBJECT TERMS (Continue on reverse if necessary and identify by block number)
FIELD	GROUP	SUB-GROUP	

19. ABSTRACT (Continue on reverse if necessary and identify by block number)

Two means are examined whereby the operations of KMR during mission execution may be improved through the introduction of advanced signal processing techniques. In the first approach, the addition of real time coherent signal processing technology to the FPQ-19 radar is considered. In the second approach, the incorporation of the MMW radar, with its very fine range precision, to the MMS system is considered. The former appears very attractive and a Phase II SBIR has been proposed. The latter does not appear promising enough to warrant further development.

DISTRIBUTION STATEMENT A:
APPROVED FOR PUBLIC RELEASE: DISTRIBUTION IS UNLIMITED.

20. DISTRIBUTION/AVAILABILITY OF ABSTRACT	21. ABSTRACT SECURITY CLASSIFICATION
☒ UNCLASSIFIED/UNLIMITED ☐ SAME AS RPT. ☐ DTIC USERS	
22a. NAME OF RESPONSIBLE INDIVIDUAL: Stanley D. Cottrill	22b. TELEPHONE (Include Area Code): (714) 894-2206 / 22c. OFFICE SYMBOL: N/A

DD Form 1473, JUN 86 — Previous editions are obsolete. — SECURITY CLASSIFICATION OF THIS PAGE

Phase I SBIR Final Report

Tracking Radar Advanced Signal Processing and Computing for Kwajalein Atoll (KA) Application

Contract No. DASG60-92-C-0022

CDRL A002

9 November 1992

Prepared for USASDC
P.O. Box 1500
Huntsville, Alabama

XonTech, Inc.

7711 CENTER AVENUE, SUITE 550
HUNTINGTON BEACH, CA 92647

XonTech, Inc.

ONE PACIFIC PLAZA, 7711 CENTER AVENUE, SUITE 550, HUNTINGTON BEACH, CALIFORNIA 92647, TELEPHONE (714) 894-2286, FAX (714) 892-5666

November 9, 1992

Commander
US Army Strategic Defense Command
Attn: CSSD-AT-P
Huntsville, AL 35807-3801

Attention: Mr. Ed Bird

Subject: Tracking Radar Advanced Signal Processing and Computing for Kwajalein Atoll (KA) Application, SBIR Phase I, Contract No. DASG60-92-C-0022

In accordance with the requirements of CDRL Item A002 of the subject contract, we are submitting as an attachment to this letter the Final Report.

If you have any comments or questions with respect to this transmittal, please contact the undersigned at 714 894 2286.

Stanley D. Cottrill

Stanley D. Cottrill
Principal Investigator

Attachment

cc
CSSD-AT-P/Mr. Ed Bird (2)
CSSD-KA-RH/Mr. Jack Cole
Contracts Office CSSD-CM-C*
Command Library CSSD-IM-PA (2)

* Copy of letter of transmittal only

Phase I SBIR Final Report

Tracking Radar Advanced Signal Processing and Computing for Kwajalein Atoll (KA) Application

Contract No. DASG60-92-C-0022

CDRL A002

9 November 1992

Principal Investigator: S.D. Cottrill
Analyst: R.D. Yates

Table of Contents

List of Tables

List of Figures

1.0 Introduction

This report is an examination into two means whereby the operations of KMR during mission execution may be improved through the introduction of advanced signal processing techniques. In the first approach, the addition of real time coherent signal processing technology to the FPQ-19 radar is considered. In the second approach, the incorporation of the MMW radar, with its very fine range precision, to the MMS system is considered.

The FPQ-19 radar is a high power C-band sensor with sensitivity characteristics approximately matching those of the ALCOR radar. The radar is also coherent ... a property which has not been exploited to date as a means of improving real time performance. This report develops means whereby the capability of the FPQ-19 radar to support real time missions may be greatly extended through the introduction of commercial off-the-shelf (COTS) equipment. This additional is found in the potential of the FPQ-19 radar to provide real time body motion measurements displayed both at the radar and at KMCC. In addition, the operating range of the radar can be significantly increased (eg, doubled) through the use of coherent integration. Also, the target resolving capability can be extended through the use of Doppler resolution in many cases typical to KMR missions. The proposed solutions involve principally, if not entirely, digital signal processing hardware thus avoiding the introduction of analog equipment with its calibration requirements and aging concerns. A method of implementation and integration is proposed which minimizes the impact on KMR operations and the degree of support from KMR resources.

The MMS system is a trilateration system capable of highly accurate position measurements stemming from a range-only measurement set. The MMW radar is a wideband radar producing a range measurement error smaller than that produced by the TRADEX/MMS combination. Thus the potential exists that incorporating the MMW radar into the MMS scheme may improve the overall position measurement accuracy. To approach the problem, the accuracy of the existing MMS system is determined. Then the MMW measurement accuracy is substituted for the TRADEX accuracy to observe the improvement in trilateration measurement accuracy. Only a very marginal improvement was observed. Thus no further effort was expended to determine how to implement an incorporation of MMW into MMS.

The report below is divided into two major sections. Section 2 addresses the FPQ-19 issues and Section 3 the MMS issues.

2.0 Development Potential of the FPQ-19 Radar

The FPQ-19 radar, a high power, C-band radar situated on Kwajalein Island, is an integral part of the Kwajalein Missile Range (KMR). The radar is capable of executing beacon and skin tracks on reentry vehicles launched from Vandenburg, AFB and other targets related to the national defense. It is also capable of tracking orbiting targets, aircraft, special test targets, etc. The radar is tied in with the other radars constituting KMR through a communications network to a central control point. When the upgrade of the current central control point is completed, it will be called the Kwajalein Mission Control Center (KMCC). As will be developed below, the FPQ-19 radar has the potential to improve the operations at KMCC as well as the potential to enhance its delivered data products.

The FPQ-19 radar (the radar) was constructed originally as a coherent radar. Subsequent measurements (Reference 1) have shown that this property is available to users. This property enables the radar to utilize both the amplitude and phase characteristics of the skin returns from targets to perform the following functions:

Coherent Integration wherein a sequence of returns are coherently summed to increase the pre-detection signal-to-noise ratio (SNR).

Doppler-based Target Resolution wherein targets which are not range-resolved by the narrowband waveform can be Doppler-resolved if the targets have a sufficient distribution in range rate. This capability can enhance the ability of the radar to observe pairs of targets which are passing each other as occurs in intercept missions and in situations where an RV is located within a chaff cloud.

Doppler Spectra Measurements wherein a sequence of target returns in a given range cell is Fourier transformed to yield precise measurements of the radial rate of the target and, with additional processing, to yield information about the local rotational motion of the target. The latter is of particular benefit to those concerned about the deployment of the reentry vehicle (RV).

Phase-Derived-Range (PDR) Tracking wherein the range to the target is measured from observations of the phase of the return rather than from

observations of the envelop of the return. Such PDR range measurements are several orders of magnitude more precise than envelop-based measurements.

The FPQ-19 radar has the potential to provide all the measurements found above. These measurements may be made in real time which can be collectively summarized and communicated to KMCC for real time display. Real time comparisons between actual and expected performance can be developed to aid the mission test directors to determine if the mission deployment and functions are operating nominally or, if not, how so. This can be of great benefit to test directors who must make rapid, correct decisions during the execution of complex missions. Early detection of non-nominal missions can enable the test directors to activate the correct, pre-determined contingency plans. The FPQ-19 radar, with its high power capability and proximity to KMCC, is ideally suited to prc vide this service to KMCC.

Beyond the real time functions, coherent data derived from the FPQ-19 radar may be processed during the post mission data analysis effort to realize all of the potential listed above. The sensors at KREMS are also able to provide these post mission benefits. However, the capacity of the KREMS sensors to cover complex missions is limited by the finite number of sensors with the correct frequency, bandwidth, beamwidth, etc. The addition of the FPQ-19 radar to the family of coherent KMR radars will ease the planning of time lines for complex missions. It addition, the FPQ-19 radar provides a backup source of data should a critical KREMS sensor experience some difficulty.

In summary, the FPQ-19 radar has the potential to greatly enhance KMR operations. To realize this potential, the first step is to develop a real time coherent signal processor. The system described below is well within the state-of-the-art and can be integrated with the FPQ-19 with minimal interference and minimal demand on KMR resources. The material below will 1) describe the FPQ-19 in overview terms sufficient for this study, 2) describe the coherent signal processor recommended for consideration, 3) indicate the means of integrating the processor with the FPQ-19, 4) and prescribe the system testing required to confirm mission readiness.

2.1 Study Objective

The discussion in Section 1 described the benefits available if the coherency capability of the FPQ-19 radar were exploited. The objective of this study is to indicate the path enabling the radar to provide the coherent products in real time and to record the data for subsequent post mission analysis. In detail, the objectives of this study are:

1) to provide a description of the FPQ-19 sufficient to support this study (Section 2.1);

2) to provide a concept level system design of a real time coherent signal processor capable of coherent integration and Doppler processing and the data recording required to support post mission analyses (Section 2.2);

3) to indicate the steps required to integrate the coherent signal processor with the radar (Section 2.3); and

4) to prescribe the type of system testing required to confirm the mission readiness state of the integrated coherent signal processor and radar (Section 2.4).

2.2 Description of the FPQ-19

The FPQ-19 radar was originally constructed by RCA who termed it the MIPIR radar. The brief description of the system provided below is derived from Reference 2. The radar operates over a frequency range extending from 5.4 GHz to 5.9 GHz. It has an antenna gain of 53 dB, a PRF selectable between 160, 320, and 640 pps, a selectable pulse width of 0.25, 0.5, 1.0, and 5.0 microseconds. The radar is capable of ambiguous range operation. The single pulse sensitivity is expressed as producing a 15 dB SNR on a one square meter target at a range of 600 nautical miles. Both beacon and skin tracking capability exists within the radar; since beacon returns are not appropriate for this study, there will be no further discussion of beacon capabilities. The radar is capable of tracking two targets simultaneously in range and one in angle.

A simplified block diagram of the system appears in Figure 2.2-1. The transmitter operates at a power level of approximately 3 megawatts. The transmitted signal is reflected off the target and received in the antenna microwave circuitry. The output of the microwave circuitry is a set of three signals: the sum signal, the traverse monopulse signal, and the elevation monopulse signal. These signals are applied to the RF head which is a low-noise, high-gain device that has been upgraded to provide two reference channels. The two reference channels permit two simultaneous range tracks; either can be associated with the monopulse channels for angle tracking purposes. The Frequency Synthesizer subsystem contains the transmit oscillator and three Local Oscillators (LOs). The frequency of any LO is such that a 30 MHz IF will result in the output of the RF head when a target return is mixed with the LO signal. One of the LOs is "coherent" with the transmit oscillator (same frequency base, giving a coherent phase relationship between the two signals). The other two LOs are non-coherent and are assigned as the skin and beacon Local Oscillators.

The four 30 MHz IF signals from the RF head are applied to the receiver where each is processed separately. The gain control selected for the primary reference channel is the same as that used for the angle channels. AGC is developed in the tracker and is automatically adjusted based on the signal strength of the target return.

The receiver also produces error signals that are derived from the azimuth and elevation inputs. These are applied to the servo control unit which, in turn, causes the antenna to adjust its pointing until nulls are produced in the angle channels.

Once the reference signals enter the channel, they are processed separately to allow individual target tracking. Each reference channel is "gated" by a range gate from the tracker subsystem. The gate allows only the selected video (target) to pass through the receiver. The system then tracks the selected target in range. In addition to the range gates developed for the receiver, the dual tracker generates PRF timing and a power programming control signal for the transmitter. Based on the range of the primary target, the tracker will cause part of the transmitter power output to be deflected and not radiated. The tracker also gauges the velocity and acceleration of the target to generate a Doppler offset form of automatic frequency control for the frequency synthesizer subsystem. The frequency of the transmitted signal is adjusted in anticipation of the target-induced Doppler shift such that the received signal only has a small residual offset frequency due to Doppler effects.

The two reference channel IF signals are brought to envelop detectors and to I/Q detectors. The two monopulse channel IF signals are brought to mixers which use a selected sum channel as reference. The mixer outputs are detected to provide the angle error signals. Of these six detected signals, only those resulting from the I/Q detectors are useful as inputs to a coherent processing scheme. The impact of this is that the monopulse channel signals cannot be subjected to coherent integration prior to detection. As a result, the extension of the operating range of the radar through coherent integration is limited to the two sum channels only; detection and range tracking may proceed but not angle tracking. A useful modification to consider then is the installation of I/Q detectors in the monopulse channels similar to those in the sum channels. No new design is required; instead the fabrication of the sum channel I/Q detectors and A/D conversion equipment is duplicated and installed in the receiver. This installation would permit coherent integration in all four channels thus truly extending the operating range of the radar. However, as there is much to be gained with the detectors as is, this study will concentrate solely on the development of signal processing based only on the sum channel I/Q outputs. These outputs are digitized with A/D converters and fed to the Tracking Data Processor System (TDPS). The A/D outputs form the inputs to the Coherent Signal Processor (COSIP) system which is conceptually developed below.

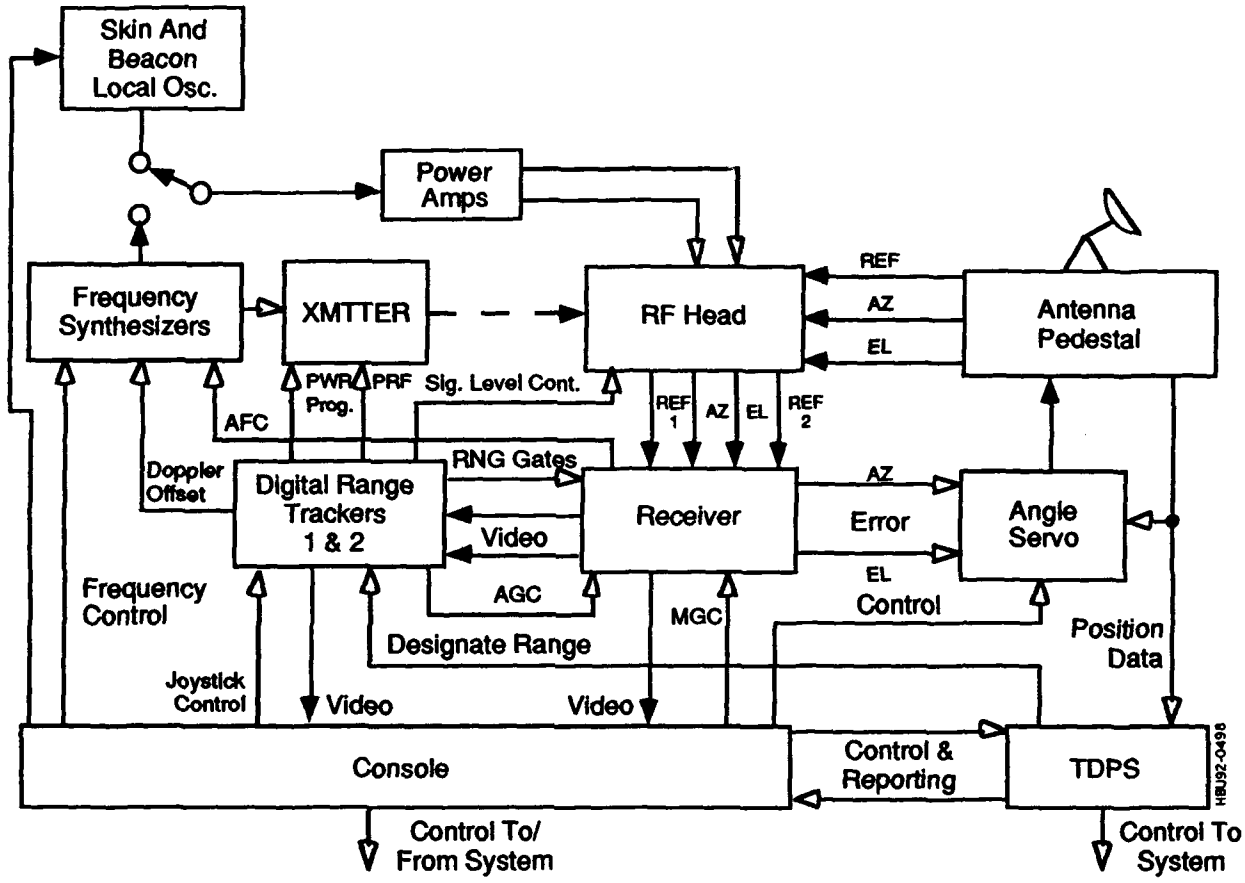

Figure 2.2-1 KMR FPQ-19, Simplified Block Diagram

2.3 Description of the Coherent Signal Processor Concept

The two sum channel A/D converter outputs are the result of coherently detecting the received sum channel signals. These A/D sequences form the input to the Coherent Signal Processor (COSIP). Figure 2.3-1 depicts an overview of COSIP which is described briefly below followed by a more thorough description. A PC is used as the host computer to provide the interface to the radar, the recording peripherals, and to house the high speed signal processing equipment. Each pulse repetition interval (PRI), a gated sequence of A/D samples is fed into two buffer memories within the PC. The Recording Buffer Memory assembles data from several PRIs into a record suitable for recording on the Data Recording device. This data is analyzed during the post mission functions. The Corner Turning Memory also assembles data over several PRIs in preparation for the real time signal processing functions. After a number of PRIs corresponding to the desired Doppler processing dwell time has expired, the output of the Corner Turning Memory is fed to the Doppler Digital Signal Processor (Doppler DSP). This device performs all the fast Fourier transform (FFT) actions and other signal processing functions required to develop the real time data displays. The output of the Doppler DSP is fed to

1) the Real Time Doppler-Based Displays which support the real time coherent integration, Doppler-based resolution, and Doppler spectra benefits of the COSIP;

2) the Display Recording which captures the real time displays on video tape for post mission playbacks;

3) a Communications Link which enables the real time displays developed at the FPQ-19 to be replicated in real time at KMCC.

The interfaces to the radar include the existing I/Q A/D samples from the two sum channels, a set of Auxiliary Data to provide time tag, encoder readings, and other digital data, and a set of timing strobes to identify receive time and the times at which the A/D data and Auxiliary Data are available for capture. As is evident, there is no penetration into the radar; only "taps" on existing signals is required. This approach enables the COSIP to be interfaced with the radar with minimum interference. Also,

COSIP may be disconnected to facilitate any possible troubleshooting exercises during integration.

The material above presented COSIP in an overview manner; next, selected elements of COSIP will be described in additional detail along with their top level performance characteristics. Described will be the recording path, the Corner Turning Memory, and the Doppler DSP. No discussion is provided for the Real Time Doppler Display and Display Recording hardware as they are composed of standard PC products.

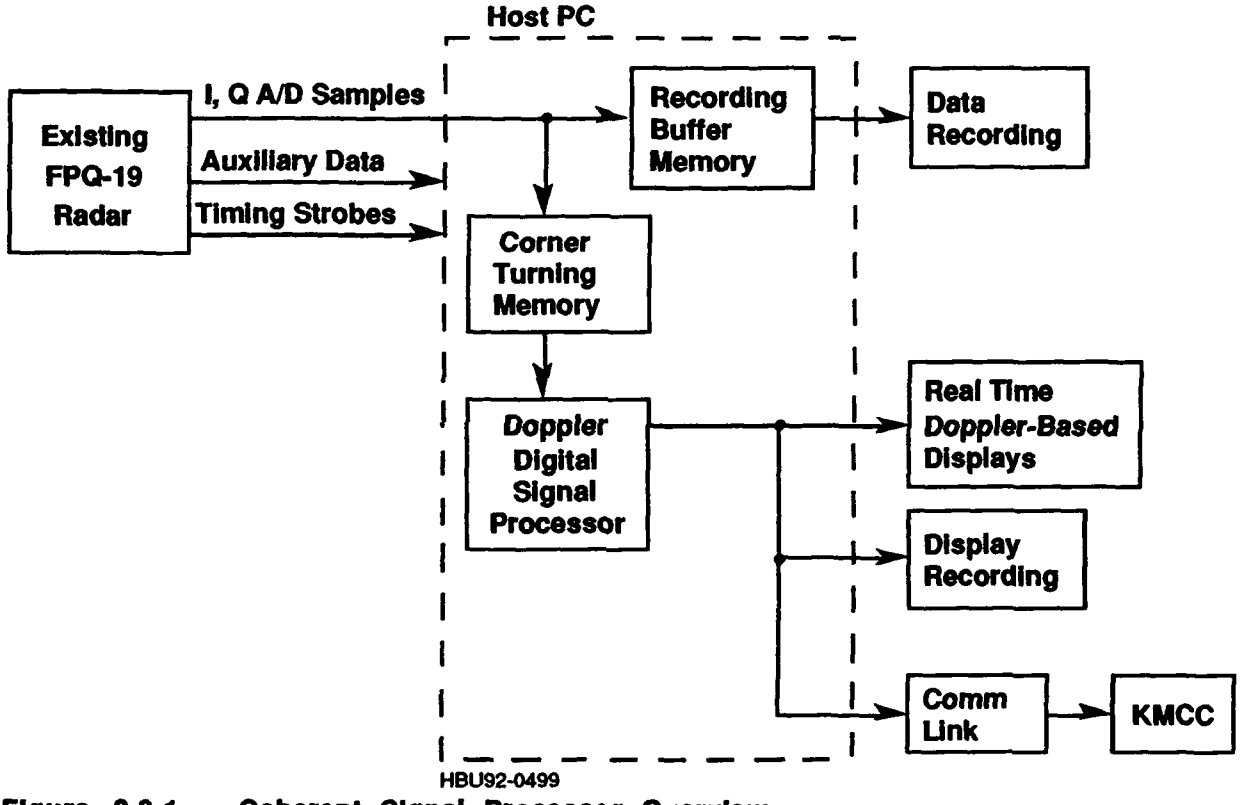

Figure 2.3-1 Coherent Signal Processor Overview

2.3.1 Data Recording Path

A critical design parameter is the required data recording rate. This is developed as follows. The development will be based on the use of a PRF of 160 pps and a pulse width of 5 microseconds. Reference 1 does not provide information as to the rate at which the A/D encoders operate. It will be assumed here that the encode rate is sufficiently high to accommodate the spectral width of the 5 microsecond pulse. If not,

separate A/D encoding may have to be included within the COSIP. The spectrum of a 5 microsecond pulse has nulls every 0.2 MHz. The sampled spectrum will be assumed to exist at least to the second nulls of the 5 microsecond pulse to capture essentially all of the signal energy and to allow a reasonable amount of spectrum space for residual Doppler shifts. Hence, the spectrum to be captured extends 0.4 MHz in each direction about DC for a total width of 0.8 MHz. An A/D encode rate of 1.0 MHz will be assumed for purposes of this report. From Reference 1, it appears that the TDPS can accommodate an A/D word length of 14 bits. While this does not quite imply that the A/D actually delivers 14 bits, it certainly constitutes a conservative assumption.

The data to be recorded each PRI will exist over a specified data window length. Experience with Kwajalein missions would indicate that a 15 Km window should suffice. The ALCOR window length for its narrowband window is approximately 2.5 Km. A 15 Km data window length corresponds to 100 microseconds in time. Over this time interval the A/D, running at 1 MHz, will produce 100 samples for each of the two channels for a total of 200 samples. As each sample is comprised of 14 bits of I-data and 14 bits of Q-data, the number of bits to be recorded per PRI is 5,600 bits or approximately 700 eight-bit bytes. The Auxiliary Data will also need to be recorded each PRI along with the A/D data. A quantity of 256 auxiliary data bytes has proven more than adequate on several KMR radars. Thus adding the 256 auxiliary data bytes to the 700 bytes of A/D data yields a total of 956 bytes of data required to be recorded each PRI. Since the radar is operating at a PRF of 160, the recording rate requirement is then 152,960 bytes/second, or approximately 200 KBytes/Second. This rate is easily accommodated by a variety of current commercial off-the-shelf optical disk and DAT tape drives. Indeed, an extension of the PRF to 320 could also be accommodated provided the pulse length remained at 5 microseconds.

2.3.2 Corner Turning Memory

The need for a "Corner Turning Memory" is developed as follows. Concentrating on a single coherent sum channel, each PRI a sequence of A/D samples is collected. Each sample corresponds to a position in range, i.e. a range cell; the entire sequence constitutes the range window over which data are processed. Thus, for the first PRI in a coherent processing dwell of N-PRIs, one can imagine the sequence of A/D samples filling up the first row in a rectangular array of buffer memory space. As the PRIs proceed, successive rows of buffer memory are filled until all N rows are filled for the

dwell. The rectangular array of memory space thus has rows corresponding to PRIs and columns corresponding to range cells. In order to perform the Doppler Fourier transforms across the number of PRIs constituting the dwell, separate FFTs must be performed for each of the range cells. Thus the data are read in from the A/D into the rows and read out of the columns into the Doppler DSP, i.e., a "corner turning". The memory is built specially for the application as the PC memory is not suitable. The size of the memory may be estimated as follows. The number of columns corresponds to the number of A/D samples each PRI. As noted above, there are a total of 200 samples. The number of rows corresponds to the number of PRIs constituting a single dwell, multiplied by two to permit double buffering. Double buffering is generally required in order to allow one dwell's worth of data to be read into the memory while the previous dwell's worth of data is being processed. The number of PRIs is the PRF times the dwell time. For missile motion analysis, a maximum dwell time of 2 seconds has sufficed in the past. Hence, the maximum number of PRIs in a single dwell is 320; the double-buffered memory must accommodate 640 PRIs. The grand total number of samples to be stored in the memory is thus 128,000. As each sample is comprised of 14 bits, the buffer memory size may be stated as 1,792,000 bits or 224 KBytes which is small by today's standards. A reasonably sized buffer may be 1 MByte which would support a dwell time of eight seconds rather than the two seconds suggested here. Alternatively, some missions may require a PRF higher than 160. A 1 MByte memory could accommodate the combination of a PRF of 320 and dwell time of over four seconds. In any case, there is ample room for generous trade-offs between PRF and dwell time.

The output of the Corner Turning Memory is fed into the Doppler DSP which is described below.

2.3.3 Doppler Digital Signal Processor

In the discussion that follows, the utilization of the DSP will be described (Section 2.3.3-1 followed by a brief description of a hardware implementation of the DSP.

2.3.3.1 Utilization of the Doppler DSP

The requirement to perform coherent integration, Doppler-based resolution, and measure target Doppler spectra all require the execution of Fourier transforms on the

columns of the Corner Turning Memory I/Q data containing the target return. For short ranges where the target location is known due to its high signal-to-noise (SNR) ratio, only those columns containing the target return need to be processed. However, at long ranges the SNR may be below zero dB and hence knowledge of the column containing the target return may be denied. In many instances typical to KMR missions, the exact location of the target may not be known early in the mission; also its velocity may not be known exactly. In order to process the returns coherently, they must stay within a single range and Doppler cell over the dwell time. Even when the target is not visible, the range window is moved along an expected (nominal) trajectory which generally suffices to maintain the target in a single 5 microsecond cell which has a width of 750 meters. In addition, at the long ranges where SNR is a problem, the target range accelerations are small which means that the target will remain in a single Doppler cell provided the premission range rate information is utilized. The latter is called motion compensation. Motion compensation is achieved by using the premission values of target trajectory to compute an expected phase shift of the target return. This phase shift is then applied to the column of I/Q samples prior to attempting any coherent processing. The resultant motion compensated column of I/Q data will possess a nearly linear phase progression which is suitable for coherent processing. The application of the motion compensation phase shift will be accomplished in the Doppler DSP. The knowledge of nominal mission trajectories will be incorporated in the host PC program which will also compute the requisite motion compensation phase shift quantities.

The Doppler DSP functions then proceed as follows. The first column of I/Q data is read out of the Corner Turning Memory into the Doppler DSP. The DSP applies motion compensation phase corrections to the sequence of I/Q samples and then performs an FFT over the samples constituting the dwell. The output of this FFT is stored in a separate memory which again is visualized as a rectangular array. The FFT data are stored in the first column which corresponds to the first column of the Corner Turning Memory, i.e., the first range cell. The process is repeated over all the columns of the Corner Turning Memory. The resultant rectangular memory formed at the output of the FFT process has columns corresponding to range cell number and rows corresponding to Doppler frequency shift. This is commonly called an image, in this case a narrowband image since the transmitted signal bandwidth is only approximately 200 KHz. The generation of this image is the principal function of the Doppler DSP. The data contained in the image will support the Doppler-based functions as indicated below.

The first function to be considered is the coherent summation of the target return to aid in the detection of weak signals. The target return will exist at some, perhaps unknown, Doppler frequency. The sequence of target returns captured during the dwell will sum coherently at a frequency corresponding to the residual target Doppler frequency. The span of frequencies represented by the image is limited to the radar PRF. If the residual Doppler frequency exceeds that span, the returns will still sum up somewhere within the image; the indicated frequency (ambiguous Doppler) will be incorrect by some multiple of the PRF. Hence, the coherently integrated target return is detected by first searching the image for the peak amplitude target and then subjecting that peak to a detection threshold test. The column of the target thus detected provides a measure of the target range. The Doppler shift of the target is determined by combining the row number (apparent frequency) of the detected target with a range rate estimate based on a sequence of range returns to eliminate the Doppler ambiguity. Range tracking may proceed based on the image response. Experience with similar radars and targets indicates that coherent summations of 16 pulses requiring only 0.1 seconds can be executed successfully. Such a summation provides a doubling of the detection range of the radar. This is a significant enhance to the radar's capability.

The second function to be considered is the resolution of targets based on Doppler resolution. The scenario here is that more than one target may exist in a single range cell and hence may be mis-identified as a single target. A single range cell has a resolution of approximately 750 meters for the 5 microsecond pulse (and 40 meters for the short 0.25 microsecond pulse). This is plenty of room in which to place two or more targets. Clutter due to rain, ground reflections, or chaff may also mask a desired target. However, if the Doppler shift of the several targets is sufficiently different, then the targets will appear as peaks in the image separated along the Doppler dimension (rows of the image rectangular array). As an example, consider two equal radar cross section targets collocated in range but with differing range rates. The question is posed then "What is the minimum range rate difference such that they are Doppler resolved". For the case of a two second dwell, the Doppler resolution is approximately the reciprocal of the dwell time, 0.5 Hz in this example. Such a Doppler frequency difference is generated by two targets with a relative range rate of 13 millimeters/second. This is a very small range rate difference and can be expected to occur frequently. The two targets collocated in range will have to move approximately

375 meters to be range resolved. If they are separating at the aforementioned 13 millimeters/second rate, they will require 480 minutes to become range resolved! While this example is extreme, it does illustrate that Doppler resolution may well succeed where range resolution fails. The performance of the FPQ-19 radar is greatly enhanced when equipped with this Doppler resolution capability. Targets resolved in Doppler are resolved just as surely as if they were resolved by a wideband radar providing range resolution. Measurements of radar cross section, trajectory, etc. may all proceed based on the Doppler-resolved target.

The third function to be considered is that of measurement of the spectrum of the target return. The spectrum of the target is found along the column of the image corresponding to the range cell containing the target return. For a simple sphere-like target, the spectrum shape will be a single peak surrounded by sidelobes. The amplitude of these sidelobes due to the finite-length dwell time may be attenuated through the use of appropriate weighting functions (Hamming, Kaiser, Taylor, etc.). This weighting will reduce the Doppler resolution and signal amplitude by predictable amounts. Trade-offs are available between the degree of sidelobe attenuation and the degree of signal resolution and amplitude loss. A more complex target which more closely represents the targets of concern to KMR may be modeled by a cone with a spherical tip, a truncated base, and a pair of rotating scatterers due to beacon antennas. The target motion may be represented as a spinning top with spin and precession frequencies. Typically the spin period will be considerably shorter than the precession frequency. Thus, to observe spin, a short dwell time is required; a long dwell will show precession better. When the target is at short ranges with adequate SNR, the Doppler DSP should process the data with both short and long dwells to highlight both spin and precession. Conversely, when the target is at long ranges with low SNRs, the short dwell time required for spin motion may not produce sufficient integration to detect the target. In this case, the Doppler DSP should be set to process long dwell intervals. The location of the target return in the image will depend on its spin and precession frequencies.

The fourth function to be considered is that of Phase-Derived-Range (PDR) Tracking wherein the range to the target is measured from observations of the phase of the return rather than from observations of the envelop of the return. Such PDR range measurements are several orders of magnitude more precise than envelop-based measurements. To perform such tracking, it is necessary to extract the measured

phase to the target each PRI (or dwell, if possible). The sequence of phase measurements thus formed will be highly ambiguous in that many multiples of 360 degree phase shift will occur between PRIs which are not observed by the radar. This ambiguity is removed to the extent that changes in range motion may be accurately measured from phase measurements. To remove the phase ambiguities, one is required to compare tracks of range as measured by phase and tracks of range as measured by the arrival time of the envelop of the target return. Alternatively, once the track is initiated, the ambiguities may be removed by bootstrapping from the history of phase measurements. Observation of the target Doppler shift may also aid the initialization process; one must be certain to remove the Doppler ambiguities properly. Generally this is not a difficult task. The phase track thus derived forms a very accurate measurement of the target range. This is because the wavelength of the C-band signal is on the order of 5 cm. This technique is occasionally threatened if there are several competing scatterers on the target. However, PDR has been successfully applied to KMR targets during post mission data analysis exercises. The extension of that analysis technique to real time application has not been developed for the FPQ-19 radar. While such may be possible, it is not part of this study.

2.3.3.2 Hardware Implementation of the DSP

The successful implementation of the Doppler DSP function will require a high speed Fourier transform device to support all the Doppler spectrum calculations. Such a device has been recently developed by Catalina Research, Inc. of Colorado Springs, CO. Under a separate contract, Catalina has developed a high speed DSP board, termed the CRV1M40, which plugs into a PC. Originally the board was developed for installation into a VME cage. The CRV1M40 is a high performance Digital Signal Processor board optimized for block oriented DSP algorithms and multi-point processing. The CRV1M40 uses a second generation high performance DSP product family. The latest technology includes a 24-bit processor implemented with radix-2, radix-4, and radix-16 algorithms yielding speed improvements of a factor of two with increased dynamic range to 24 bits (144 dB).

A single CRV1M40 DSP board can execute a 1,024 complex-point FFT in 80.7 microseconds. Systems can be configured with cascaded or parallel boards offering increased processing performance. The CRV1M40 can perform real time digital filtering, image recognition, image compression, correlation, convolution, spectrum

analysis, matrix operations, complex FIR filters, and adaptive filtering in either the time domain or the frequency domain. Various memory modules are available for processing data array sizes up to one million points. FIFO modules are available for systems requiring real time continuous data.

The board has been developed for VME and PC applications with a clock speed of 40 MHz. A port separate from the PC bus is available for high speed data transfers into and out of the board. The PC version of the board is currently under final testing leading to production models.

2.4 Conceptual Integration of the COSIP with the FPQ-19

The COSIP can, and should be fabricated and unit tested as a stand-alone device prior to shipment to KMR. The A/D input from the radar can be simulated with buffer memories as can the Auxiliary Data. The timing strobes can be simulated with test equipment. The Data Recording device, the Real Time Doppler-based Displays, and the Display Recording can all be tested in CONUS. The Communication Link can be partially tested in CONUS.

The radar outputs including the A/D sample sequence, the Auxiliary Data, and Timing Strobes can all be developed at KMR during the COSIP fabrication and CONUS test time interval. An Interface Control Document should be maintained to insure that proper electrical and mechanical interfaces are developed on both sides of the interface.

Upon successful completion of CONUS testing and the FPQ-19 interface boundary, the COSIP would be shipped to KMR for attachment to the FPQ-19. The interfaces should all be based on durable connectors thus permitting rapid disconnect as required to maintain operational status of the radar as required. Pre-connection tests should be conducted to insure that neither the radar or COSIP equipment will be damaged upon connection. Immediately after connection, diagnostic tests should be conducted on the radar to insure that the COSIP produced no deleterious effects on the radar. Following successful completion of those tests, predictable A/D and Auxiliary Data blocks should be passed from the radar to COSIP to confirm proper interfacing.

2.5 Integrated System Testing

Once the COSIP has been successfully integrated into the radar, system tests should be conducted to verify the radar's operational status, that COSIP is performing to specifications, and to insure that the radar is producing the expected data and data quality.

To verify the radar's operational status, it is recommended that the radar conduct its normal countdown tests twice: once with COSIP connected to show that COSIP produces no bad effects, and once with COSIP disconnected to show that disconnecting COSIP returns the radar to its pre-COSIP state.

The initial tests to be conducted to show that COSIP and the radar are performing according to expectations can be based on the local horn test target mounted near the radar. This target is very handy in that it is always present on demand. These tests will serve to confirm the proper transfer and content of the Auxiliary Data and the proper timing and adequacy of the Timing Strobes (see Figure 2.3-1). A preliminary check on the A/D transfers is also possible with this test target. When the utility of the local test target has been exhausted, orbiting calibration spheres should be tracked as they are ideal radar backscatterers and their trajectories may be accurately predicted permitting effective motion compensation. Initially the radar should be fully calibrated and the sphere tracked to show that COSIP is capable of observing the correct radar cross section and trajectory. Subsequently, data on the orbiting sphere should be recorded and processed to show that coherency does exist and to measure its quality. Quality measures will include measures of the Doppler sidelobes and pulse-to-pulse RMS phase jitter. When the radar/COSIP system is shown to be coherent, additional real time tracks of orbiting spheres should be conducted to confirm the generation of the real time Doppler-based displays and display recording.

All such test procedures should be carefully documented to form the basis of a site COSIP operation and maintenance manual. In addition, training sessions conducted by COSIP personnel should be provided to familiarize the site personnel with the operation and maintenance of COSIP.

3.0 Incorporation of MMW in MMS Trilateration Measurements

In this section the effect of incorporating the MMW (Millimeter Wave) radar into the MMS (Multistatic Measurement System) is presented. A brief description of the system parameters are given followed by the range and angle measurement error models used in this study. The trilateration equations are given and a first order error analysis developed. The single pulse measurement errors of the target's xyz position along a simplified trajectory are computed and used to characterize the system performance. The performance is computed both for an envelope derived range measurement and a phase derived range measurement. The TRADEX radar is then replaced by the MMW radar for the computation of the monostatic range to the target and the process was repeated. For comparison purposes the errors in determining the target's xyz position is also computed based only on the monostatic range, azimuth and elevation measurements for the TRADEX and MMW radars. A first order error model for the xyz position in terms of the range, traverse and elevation angle estimates is used for this purpose. The basic result is that incorporating the MMW radar range measurement into the MMS system offers a marginal improvement in the estimate of the target's xyz position for either envelope or phased derived range measurements. It is also noted that the MMW monostatic envelope derived range and monopulse angle measurements provided target position errors that were at least as good as the MMS errors based on envelope derived range measurements. However, when the target characteristics allowed the MMS system to use a phase derived range measurement at each sensor, the MMS performance was far superior to the MMW monostatic measurement performance.

3.1 System Descriptions

The L-Band MMS (Multistatic Measurements System) consists of two bistatic receiver systems located on the islands of Gellinam and Illeginni in the Kwajalein Atoll. Two microwave link systems allow control and communication with the KREMS radar TRADEX, located on Roi-Namur as well as real time metric calibration and timing of the remote sites. As shown in Figure 3.1-1, from Ref [3], TRADEX illuminates the target and points the remote antennas. The bistatic stations then receive the target returns and transmit the data back to TRADEX via the link for recording and coherently processing the three station measurements. A complete description of the MMS system is contained in Ref.[3], while the trilateration tracker is presented in Ref. [4].

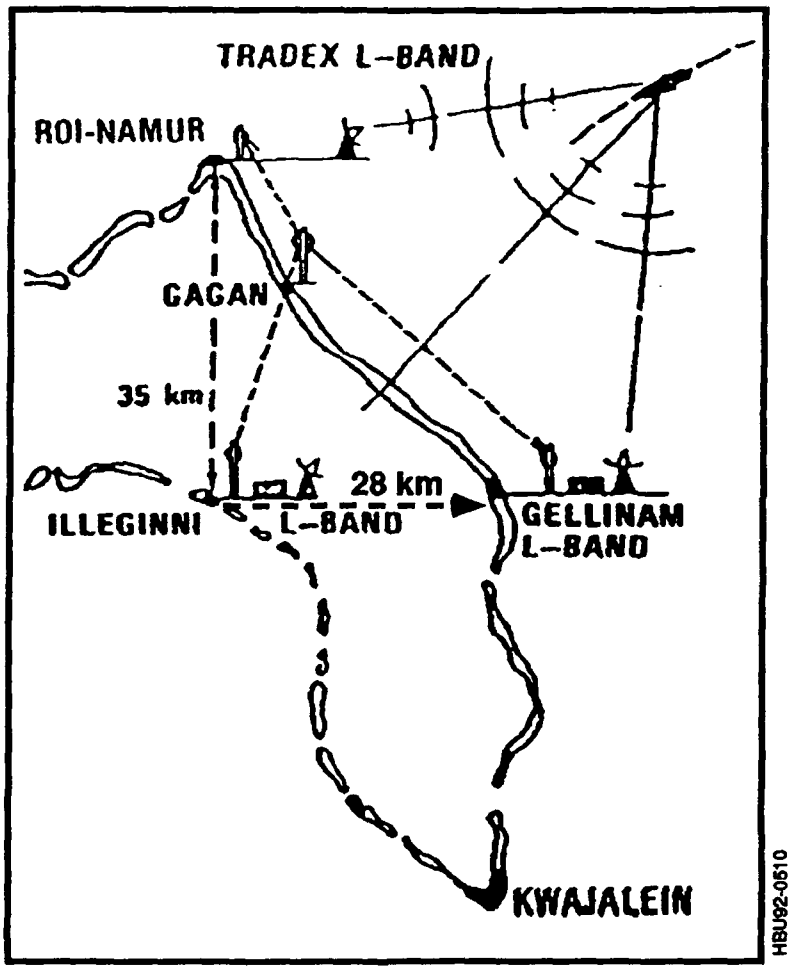

Figure 3.1-1 Overall Layout of the Multistatic Measurement System at USAKA

The TRADEX Radar is described in Ref. [5], while the MMW (Millimeter Wave Radar) is described in Ref [6]. A complete overview of the latest radar parameters may be found in Ref. [7].

A summary of the L-Band MMS system parameters are given in Table 3.1-1. It is seen that the waveforms used consist of a 50 microsecond 20 MHz LFM (Linear Frequency Modulated) pulse, and a 32 pulse burst consisting of 2 microsecond 20 MHz LFM pulses. The 6 dB width range resolution is 15 meters. The SNR (signal-to-noise ratio) for a 0 dBsm target at a range of 120 Km is 55.4 dB for the pulse mode and 55.9 dB for the burst mode. The TRADEX radar has a one way 3 dB beamwidth of 10 milliradians and a SNR for a 0 dBsm target at a range of 120 Km of 66.8 dB for the pulse mode and

67.3 for the burst mode. Note that the TRADEX receiver is 11.4 dB more sensitive than the two MMS receivers. This is mainly due to the smaller antenna used at the remote sites.

Table 3.1-1 Multistatic Measurement System (MMS) Parameters

Carrier Frequency:	1320 GHz
Waveform:	
Pulse Train:	
Pulse Length	50 μsec
Chirp Excursion	20 MHz
PRF	100-1500 (Hz)
Burst:	
Pulse Length	2 μsec
Chirp Excursion	20 MHz
Number Pulses	32
Range Resolution: (6 dB Width)	15 Meters
Tradex Beamwidth: (One Way 3 dB Width)	10 (mrad)

Sensitivity:
SNR on a 1m Target at a 120 Km Range

Waveform	MMS	Tradex
Pulse	55.4 dB	66.8 dB
Burst	55.9 dB	67.3 dB

A summary of the MMW radar system parameters are given in Table 3.1-2. Only the wideband waveform characteristics are shown. The waveform consists of a 50 microsecond 1000 MHz LFM pulse. The 6 dB width range resolution is 0.28 meters and the one-way 3 dB beamwidth is 0.760 milliradians. The SNR for a 0 dBsm target at a range of 120 Km is 56.8 dB.

Table 3.1-2 Millimeter Wave (MMW) Radar Parameters

Carrier Frequency:	35 GHz
Waveform:	
Pulse Train:	
Pulse Length	50 μsec
Chirp Excursion	1 GHz
PRF	50-2000 (Hz)
Range Resolution: (6 dB Width)	0.28 Meters
Beamwidth (One Way 3 dB Width)	0.760 (mrad)
Sensitivity: (SNR on a 1m Target at a 120 Km Range)	56.8 dB

3.2 Measurement Error Models.

In order to realistically analyze the system it has been assumed that the major error contributions arise from the measurements of the targets range to each sensor based on a time of arrival estimate of the radar pulse at each sensor. It has also been assumed that the system has been properly calibrated. The standard deviation of the envelope derived range estimate may be expressed as follows:

$$\sigma_1 = \frac{K \cdot R_6}{\sqrt{2 \cdot SNR}} \qquad (1)$$

in which SNR is the signal-to-noise power ratio, R_6 the 6 dB width range resolution, and K is a constant that depends on the range sidelobe suppression filters and the exact estimation scheme used. For a peak picking scheme and a Hamming frequency weighting of the LFM pulse for range sidelobe suppression, it can be shown that K = 0.345. (see Ref [8] for details). The SNR is defined as the ratio of the signal power to the total noise power sampled at the peak output of the range compression filter. For the case of a phase derived range estimate, it can be shown that the standard deviation is given as follows:

$$\sigma_2 = \frac{\lambda}{4\pi\sqrt{2 \cdot SNR}} \qquad (2)$$

In order to use the phase derived range measurements, the phase from consecutive radars returns has to be unwrapped unambiguously based on the velocity estimate of the target. For a point scatterer this generally requires that the velocity estimate have an error less than λ PRF/4. However, due to the 20 MHz bandwidth of the MMS waveforms, complex targets will scintillate and require a higher PRF for adequate phase unfolding. The burst waveform may be used to filter out the scintillation to some extent by sampling the peak in Doppler and using the corresponding phase. For the analysis in this study it has been assumed that the phase unfolding can be accomplished and that effects of the phase scintillation on the estimate of the range phase can be neglected.

For the TRADEX and MMW radars, the traverse and elevation angle estimates have the following standard deviations:

$$\sigma_3 = \frac{K_a \cdot \theta_3}{\sqrt{2 \cdot SNR}} \qquad (3)$$

in which θ_3 is the 3 dB width of the one-way sum beam response, and KA is a constant that depends on the monopulse beams. Based on calibration data from MMW, it can be shown that K_a = 0.5. For this study it has been assumed that TRADEX has the same constant.

3.3 Trilateration Equations

The trilateration concept is shown in Figure 3.3-1. For simplicity, it has been assumed that the TRADEX radar and the two MMS sensors are in the x-y plane, and that the xyz coordinate system is centered at the TRADEX radar antenna with x in the east direction and y in the north direction. In addition, it has been assumed that the Illeginni sensor is on the y axis and the Gellinam sensor is exactly due east of it. Hence, the TRADEX, Illeginni and Gellinam sensors have coordinates (0,0,0), (0,-B,0) and (A, -B,0), respectively where B is the range of TRADEX to Illeginni, and A is the range of Illeginni to Gellinam. A good approximation for these quantities is A=28 km and B=35 km. Although these are not the exact sensor positions, for the purposes of this study

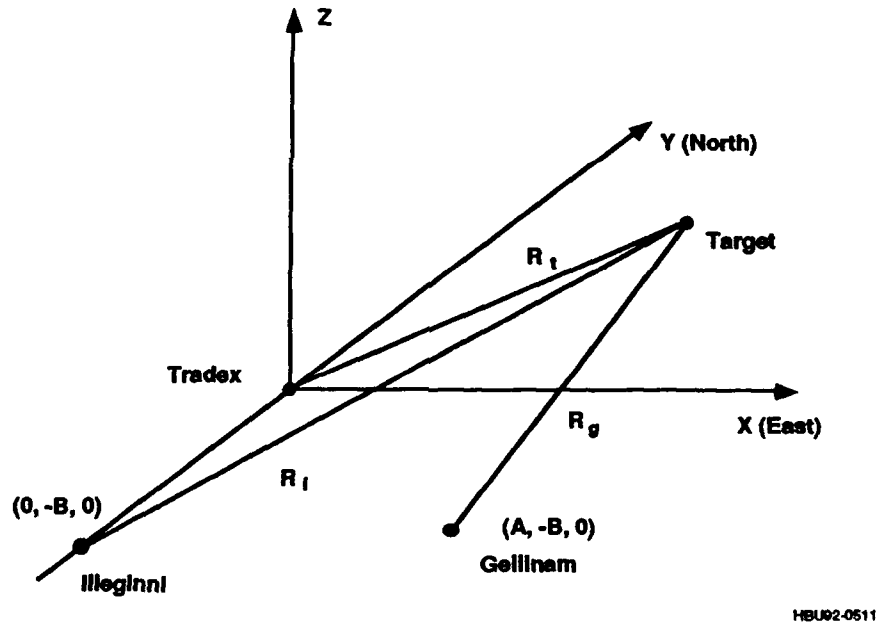

R_t: Target Range from Tradex
R_l: Target Range from Illeginni
R_g: Target Range from Gellinam

Figure 3.3-1 Trilateration Concept

these assumptions greatly simplify the trilateration equations and do not compromise the results. The three leg ranges may be expressed in terms of the targets xyz coordinates as follows:

$$R_t = \sqrt{X^2 + Y^2 + Z^2} \tag{4}$$

$$R_i = \sqrt{X^2 + (Y+B)^2 + Z^2} \tag{5}$$

$$R_g = \sqrt{(X-A)^2 + (Y+B)^2 + Z^2} \tag{6}$$

The equation can then be used to solve for the target's X, Y, Z coordinates in terms of the ranges as follows:

$$X = \frac{R_i^2 - R_g^2}{2A} + \frac{A}{2} \tag{7}$$

$$Y = \frac{R_i^2 - R_t^2}{2B} - \frac{B}{2} \tag{8}$$

$$Z = \sqrt{R_t^2 - X^2 - Y^2} \tag{9}$$

in which R_t , R_i and R_g are the (leg)ranges to the target from the TRADEX, Illeginni and Gellinam sensors respectively. The corresponding total monostatic and bistatic time delays can be expressed in terms of theses ranges as follows:

$$\tau_t = \frac{2\,R_t}{c} \tag{10}$$

$$\tau_i = \frac{R_t + R_i}{c} \tag{11}$$

$$\tau_g = \frac{R_t + R_g}{c} \tag{12}$$

in which c is the speed of light. Based on these equations, given the measurements of the time delays, the ranges can be estimated as follows:

$$\hat{R}_t = \frac{c}{2}\,\hat{\tau}_t \tag{13}$$

$$\hat{R}_i = c\,\hat{\tau}_i - \frac{c}{2}\,\hat{\tau}_t \tag{14}$$

$$\hat{R}_g = c\,\hat{\tau}_g - \frac{c}{2}\,\hat{\tau}_t \tag{15}$$

These range estimates can then be substituted into equations (7), (8), (9) to form the estimate of the targets position, based on a single transmission.

In order to compute the mean and variance of the position estimates, one can expand the equations for x, y and z to first order as a function of the time delay measurement errors as follows:

$$\hat{x} = x + \Delta x \tag{16}$$
$$\hat{y} = y + \Delta y \tag{17}$$
$$\hat{z} = z + \Delta z \tag{18}$$

$$\Delta x = KXT \cdot \Delta\tau_t + KXI \cdot \Delta\tau_i + KXG \cdot \Delta\tau_g \tag{19}$$
$$\Delta y = KYT \cdot \Delta\tau_t + KYI \cdot \Delta\tau_i + KYG \cdot \Delta\tau_g \tag{20}$$
$$\Delta z = KZT \cdot \Delta\tau_t + KZI \cdot \Delta\tau_i + KZG \cdot \Delta\tau_g \tag{21}$$

$$\tau_t = \hat{\tau}_t - \tau_t \tag{22}$$
$$\Delta\tau_i = \hat{\tau}_i - \tau_i \tag{23}$$
$$\Delta\tau_g = \hat{\tau}_g - \tau_g \tag{24}$$

The gain factors K • • correspond to the partial derivatives of the positions with respect to the measurements, and are given as follows:

$$KXT = \frac{\partial X}{\partial \tau_t} = \frac{R_g - R_i}{A} \cdot \frac{c}{2} \tag{25}$$

$$KXI = \frac{\partial X}{\partial \tau_i} = \frac{R_i}{A} \cdot c \tag{26}$$

$$KXG = \frac{\partial X}{\partial \tau_g} = -\frac{R_g}{A} \cdot c \tag{27}$$

$$KYT = \frac{\partial Y}{\partial \tau_t} = -\frac{R_t + R_i}{B} \cdot \frac{c}{2} \tag{28}$$

$$KYI = \frac{\partial Y}{\partial \tau_i} = \frac{R_i}{B} \cdot c \tag{29}$$

$$KYG = \frac{\partial Y}{\partial \tau_g} = 0 \tag{30}$$

$$KZT = \frac{\partial Z}{\partial \tau_t} = \left(\frac{R_t}{Z} + \frac{Y}{B}\frac{R_t + R_i}{Z} + \frac{X}{A}\frac{R_i - R_g}{Z} \right) \cdot \frac{c}{2} \tag{31}$$

$$KZI = \frac{\partial Z}{\partial \tau_i} = -\left(\frac{X}{A} + \frac{Y}{B} \right) \frac{R_i}{Z} \cdot c \tag{32}$$

$$KZG = \frac{\partial Z}{\partial \tau_g} = \frac{X}{A}\frac{R_g}{Z} \cdot c \tag{33}$$

The above equations may be used to compute the mean value (bias) and standard deviation of the position errors Δx Δy Δz in terms of the delay estimate errors $\Delta\tau_t$, $\Delta\tau_i$, and $\Delta\tau_g$.

The position biases will depend on the time delay biases, and are magnified by the various partial derivative terms. This results in the GDOP (geometric dilution of position) effect. This term will not be considered further since it is not a function of the time delay variances.

The standard deviation of the time delays can be expressed in terms of the radar range estimation errors , given by Eq. (1) (envelope range) or Eq (2) (phase derived range) as follows:

$$\sigma_{\Delta\tau} = \frac{2}{c}\ \sigma_{\Delta R} \tag{34}$$

It is illuminating to compare the MMS estimate of the target's position to that obtained by a monostatic radar using the measurements of range, azimuth and elevation. The radar coordinate system is show in Figure 3.3-2. The xyz position may be expressed in terms of the range , azimuth and elevation angles as follows:

$$x = R\ \cos E\ \sin A \tag{35}$$

$$y = R\ \cos E\ \cos A \tag{36}$$

$$z = R\ \sin E \tag{37}$$

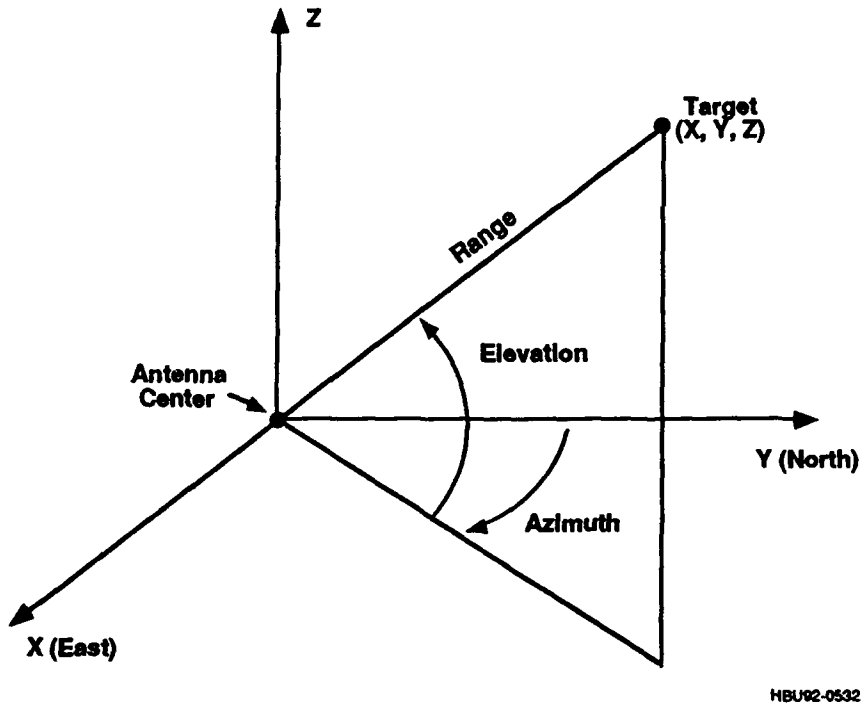

Figure 3.3-2 Radar Coordinate System

Given that the antenna boresite is pointing at an azimuth of A_0 and an elevation of E_0, and that the traverse and elevation monopulse angles measurements are given by ΔT and ΔE, the target azimuth and elevation angles for a target near boresite may be computed as follows:

$$E = E_0 + \Delta E \tag{38}$$

$$A = A_0 + \Delta T / \cos E_0 \tag{39}$$

Using the above equations, the estimate of the target's xyz position may be expressed to first order in terms of the traverse and elevation monopulse errors as follows:

$$\hat{x} = x + \Delta x \tag{40}$$

$$\hat{y} = y + \Delta y \tag{41}$$

$$\hat{z} = z + \Delta z \tag{42}$$

$$\Delta x = GXR \cdot \Delta R + GXE \cdot \Delta E + GXT \cdot \Delta T \tag{43}$$

$$\Delta y = GYR \cdot \Delta R + GYE \cdot \Delta E + GYT \cdot \Delta T \tag{44}$$

$$\Delta z = GZR \cdot \Delta R + GZE \cdot \Delta E + GZT \cdot \Delta T \tag{45}$$

$$\Delta R = \hat{R} - R \tag{46}$$

$$\Delta E = \hat{E} - E \tag{47}$$

$$\Delta T = \hat{T} - T \tag{48}$$

in which ΔR, ΔT and ΔE are the range, traverse and elevation measurement errors. The various gain factors are expressed in terms of the partial derivatives as follows:

$$GXR = \frac{\partial X}{\partial R} = \cos E \sin A \tag{49}$$

$$GXE = \frac{\partial X}{\partial E} = -R \cos E \sin A \tag{50}$$

$$GXT = \frac{\partial X}{\partial T} = R \cos A \tag{51}$$

$$GYR = \frac{\partial Y}{\partial R} = \cos E \cos A \tag{52}$$

$$GYE = \frac{\partial Y}{\partial E} = -R \sin E \cos A \tag{53}$$

$$GYT = \frac{\partial Y}{\partial T} = -R \sin A \tag{54}$$

$$GZR = \frac{\partial Z}{\partial R} = \sin E \tag{55}$$

$$GZE = \frac{\partial Z}{\partial E} = R \cos E \tag{56}$$

$$GZT = \frac{\partial Z}{\partial T} = 0 \tag{57}$$

3.4 Examples

In order to determine the measurement errors versus altitude, a simplified trajectory was employed and is described by Figure 3.4-1. Given an impact point in the xy plane, the trajectory is defined by an azimuth and elevation angle. Commencing at an altitude of approximately 200 km, the target is flown along the trajectory to impact. The azimuth and elevation angles were chosen to be 45 and 18 degrees respectively. The various impact points at Kwajalein are shown in Figure 3.4-2 Ref [7]. After computing the errors along the trajectories for several impact points, number 38 was selected as a representative example. Although the exact value of the errors varied as a function of impact point and the trajectory azimuth and elevation angles, they all lead one to the same conclusions. The cases studied are summarized in Table 3.4-1. The first 4

cases consider the performance of the MMS system with range measurements only. For comparison purposes, cases 5 through 8 consider a single sensor employing range, azimuth and elevation measurements.

In actual practice the MMS system trilateration Kalman filter uses the three leg ranges and the azimuth and elevation angles from the TRADEX sensor. One would then add the MMW estimates of range, azimuth and elevation to the measurements. The estimated measurement variances are used to properly weight the data for use with the trilateration filter. It was beyond the scope to this study to simulate the full trilateration filter. However, after an analysis of the measurement variances, it was felt that they could be used to generate the correct conclusions as to the system performance.

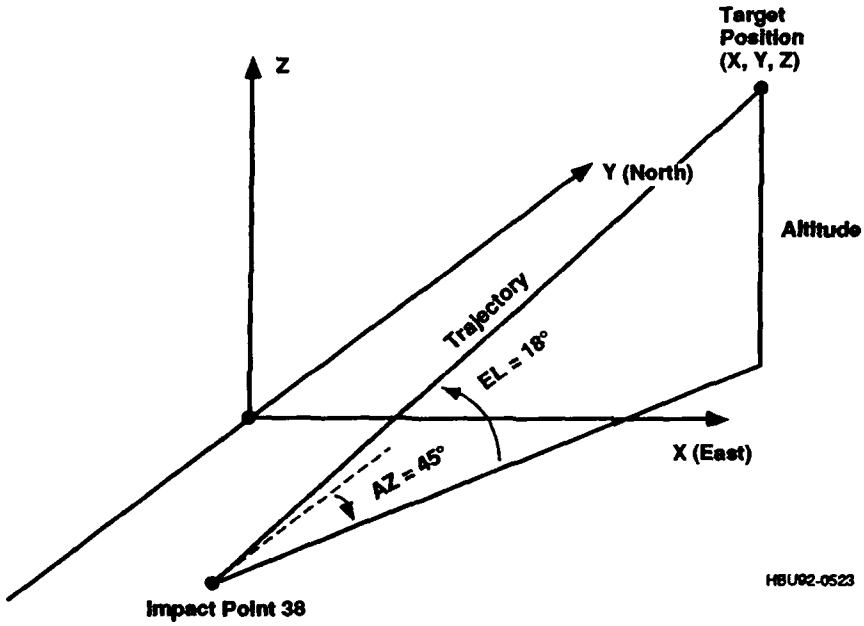

Figure 3.4-1 Target Trajectory

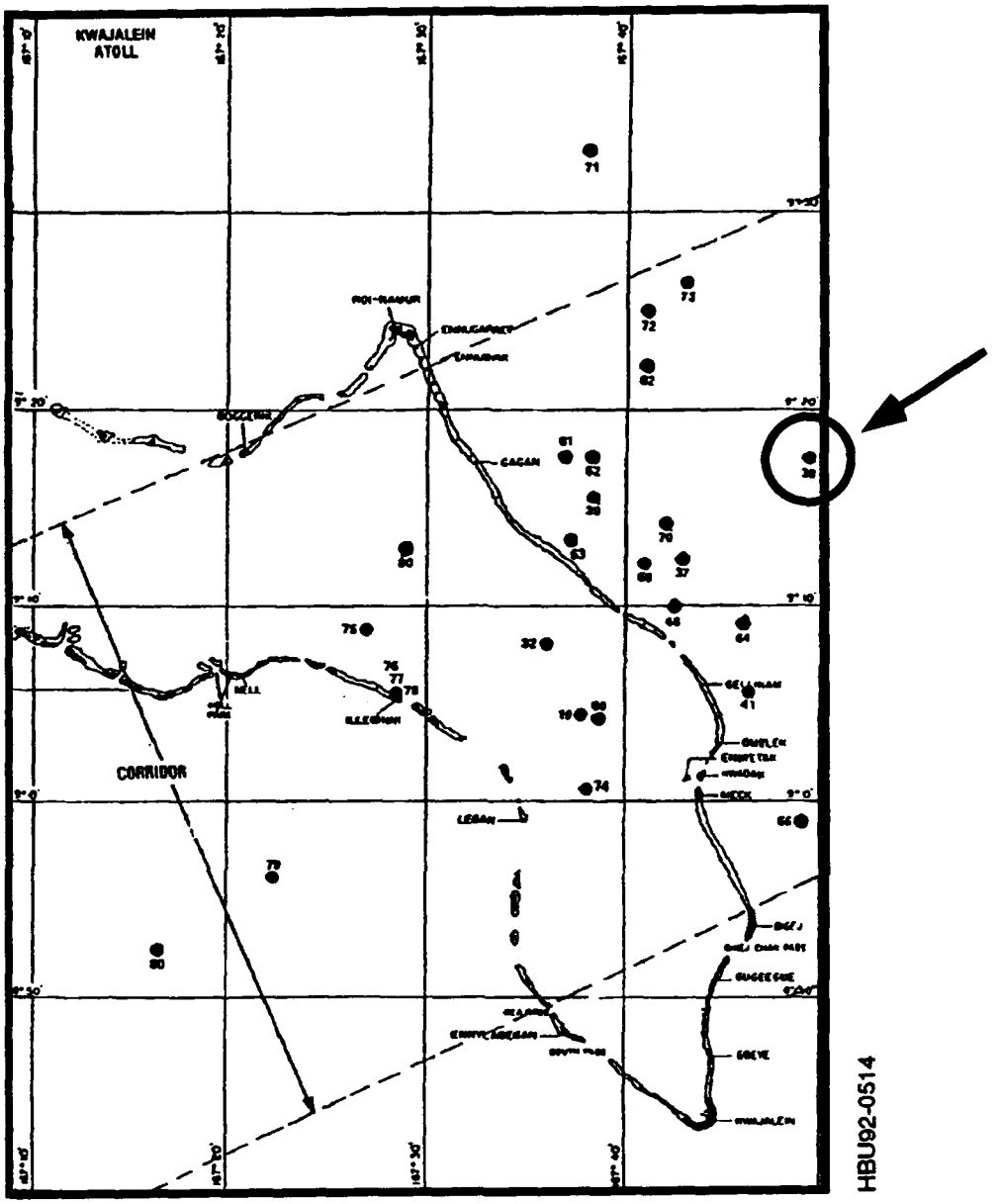

Figure 3.4-2 Target Impact Points

Table 3.4-1 Cases Studied

Case	Radar Measurements	RoI to Target Leg Sensor	No. of MMS Sensors
1	3 envelope ranges	TRADEX	2
2	3 envelope ranges	MMW	2
3	3 phase-derived ranges	TRADEX	2
4	3 phase-derived ranges	MMW	2
5	envelope range azimuth elevation	TRADEX	0
6	envelope range azimuth elevation	MMW	0
7	phase-derived range azimuth elevation	TRADEX	0
8	phase-derived range azimuth elevation	MMW	0

For cases 1 through 4 the variances of the x,y, and z position estimates were computed using Eqs. (16) through (33). The signal-to noise ratio in Eq. (1) and (2) was computed using the sensor sensitivity and was scaled as a function of the total bistatic and monostatic ranges to the target. It was assumed that the monostatic and bistatic radar cross-sections were identical. The radar cross-section was set to -25 dBsm and it was assumed that each sensor coherently integrated 32 pulses. These values were chosen to yield representative errors. In the case of phase derived range measurements, it was assumed that the biases introduced by the PDR concept were either negligible, or were estimated. Since the phase derived range processing is usually done off-line, one method for the estimation of the PDR biases is to include them as a state in the batch estimation algorithm which uses a forward and backward pass of all the data along the trajectory. For cases 5 through 8 the variances of the x,y, and z position estimates were computed using Eqs. (40) through (57).

For a practical system, the range and angle estimation errors have a quantization noise which is independent of the signal-to-noise ratio. The exact value depends on the system configuration and the algorithms employed to estimate the time-or-arrival and the monopulse angles. For this study, these effects were neglected. However, the effects can be approximated by clamping the signal-to-noise ratio when it exceeds a given value. This was done for a value of 30 db. The results obtained do not change the general conclusion of this study.

The results for cases 1 and 2 are shown in figures 3.4-3 and 3.4-4 respectively. It is seen that using the MMW radar in place of TRADEX for the computation of the envelope derived range does not significantly reduce the position errors. This can be seen in more detail from the results presented in Table 3.4-2. The percent contribution of the TRADEX and MMW sensors to the total position variance is shown for each coordinate as a function of altitude. For the example chosen, the y axis errors a most effected. It is seen that TRADEX contributes less than 5.76%, and MMW less than 0.02 %. The results are due to the fact that the position errors are driven by the time-of-arrival measurement errors of the two MMS sensors. Another way to interpret these results is to determine the reduction in the standard deviation of the position estimates under the assumption that the active sensor (TRADEX or MMW) provides an error free value for the time delay of the Roi-target path. Based on the definition of the ratio R computed in table 3.4-2, it follows that this reduction is given by $\sqrt{1-R}$. Hence, when the system includes TRADEX (noise free) plus the two MMS sensors, the standard deviation of the y position at an altitude of 120 km is reduces by a factor of 0.971 when compared to the TRADEX (noisy) plus two MMS sensors.

The corresponding results for cases 3 and 4, in which the range measurements are based on the phase-derived-range algorithm, are shown in figures 3.4-5 and 3.4-6 and table 3.4-3. Again, it is seen that the position errors are mainly driven by the MMS sensors. The TRADEX variance ratios R are identical for the envelope and phase derived range cases because the ratio of the TRADEX and MMS range measurement variances are identical for both the envelope and phased derived range measurements. However, note that the position errors are reduced by a factor of approximately $286 = \sigma_1/\sigma_2$ which is the gain due to the phase-derived range accuracy relative to the envelope range accuracy. Again, it is seen that if the time delay estimate of the Roi-target path were perfect, the standard deviation of the y axis position would be reduced by a factor of 0.971.

The position errors based only on the active sensor using the measurement of envelope range, azimuth and elevation , are shown in figures 3.4-7 and 3.4-8. On comparing figures 3.4-3 and 3.4-7, it is seen that the MMS-TRADEX system has smaller errors in the x and y positions, and a larger error in the z position, than the TRADEX only system. On comparing figures 3.4-3 and 3.4-8, it is seen that the MMS-TRADEX system has larger errors in all positions than the MMW only system. Although not all possible trajectory and impact points were studied, it is a reasonable to state that when envelope range measurements are used, the MMW system alone yields more accurate position estimates than the TRADEX-MMS system. This can be attributed to the increased range and angle accuracy of the MMW sensor.

The position errors based only on the active sensor using the measurement of phase derived range, azimuth and elevation , are shown in figures 3.4-9 and 3.4-10. On comparing figures 3.4-7 to 3.4-9, and 3.4-8 to 3.4-10, it is seen that the increased range accuracy does not significantly alter the position errors. This can be attributed to the fact that the position errors are mainly due to the angle errors times the range to the target.

It should be remarked that the narrowband L-band RCS and the wideband K_a-band RCS were assumed to be equal. This assumption does not change the conclusion with regards to the inclusion of the MMW range measurements into the MMS system. However, the conclusion that the MMW only system (envelope range, azimuth, elevation) has smaller position errors than the MMS-TRADEX system (envelope range) could be reversed if the wideband K_a-band RCS is less than the narrowband L-band RCS.

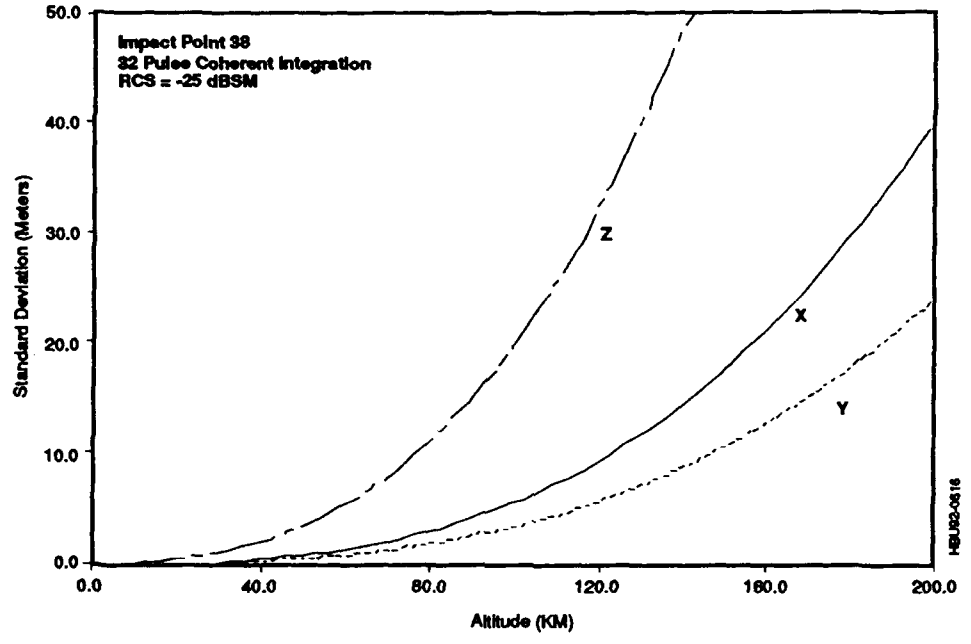

Figure 3.4-3 **Target Position Errors vs. Altitude Tradex Plus Two MMS Sensors. Envelope Range**

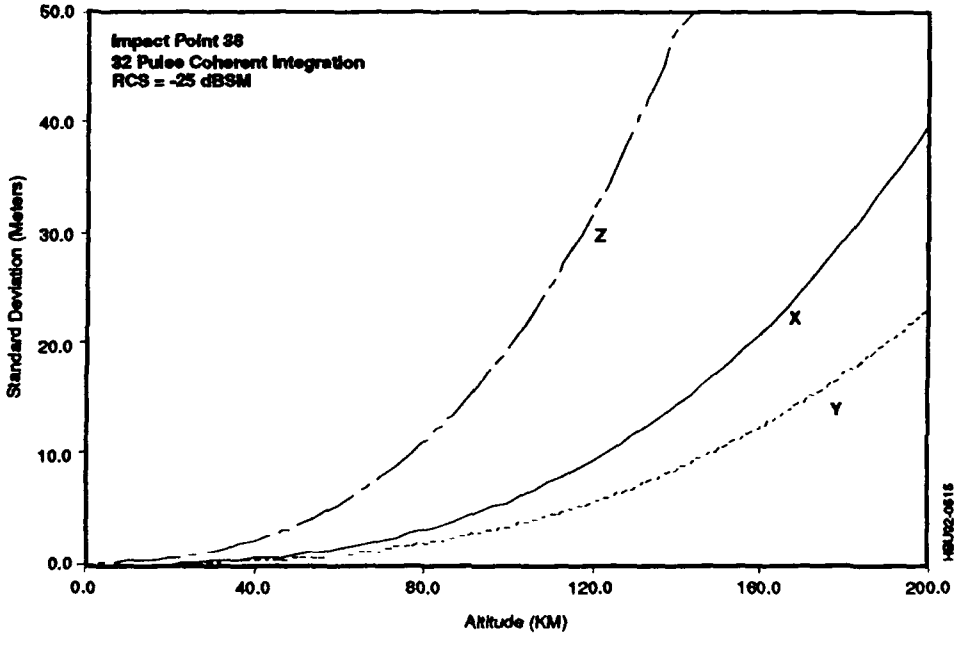

Figure 3.4-4 **Target Position Error vs. Altitude MMW Plus Two MMS Sensors. Envelope Range.**

Tradex

Alt. (KM)	R_x	R_y	R_z
120.	0.002	5.754	0.904
117.	0.002	5.732	0.900
113.	0.002	5.709	0.896
110.	0.002	5.685	0.892
107.	0.002	5.660	0.887
103.	0.002	5.633	0.883
100.	0.002	5.605	0.878
97.	0.003	5.576	0.873
93.	0.003	5.545	0.867
90.	0.003	5.512	0.862
87.	0.003	5.478	0.856
83.	0.003	5.441	0.850
80.	0.004	5.402	0.843
77.	0.004	5.361	0.836
73.	0.004	5.318	0.828
70.	0.005	5.271	0.820
67.	0.005	5.222	0.812
63.	0.005	5.169	0.803
60.	0.006	5.112	0.793
57.	0.006	5.052	0.783
53.	0.007	4.987	0.772
50.	0.008	4.917	0.761
47.	0.009	4.842	0.748
43.	0.010	4.760	0.734
40.	0.011	4.673	0.720
37.	0.013	4.579	0.704
33.	0.015	4.477	0.688
30.	0.017	4.368	0.670
27.	0.020	4.251	0.651
23.	0.024	4.128	0.631
20.	0.029	4.002	0.612
17.	0.036	3.879	0.593
13.	0.046	3.771	0.577
10.	0.062	3.705	0.569
7.	0.088	3.741	0.580
3.	0.137	4.022	0.636

$$R = \frac{\text{Tradex Variance}}{\text{Total Variance}} \times 100$$

MMW

Alt. (KM)	R_x	R_y	R_z
120.	0.000	0.021	0.003
117.	0.000	0.021	0.003
113.	0.000	0.021	0.003
110.	0.000	0.021	0.003
107.	0.000	0.021	0.003
103.	0.000	0.021	0.003
100.	0.000	0.021	0.003
97.	0.000	0.021	0.003
93.	0.000	0.020	0.003
90.	0.000	0.020	0.003
87.	0.000	0.020	0.003
83.	0.000	0.020	0.003
80.	0.000	0.020	0.003
77.	0.000	0.020	0.003
73.	0.000	0.020	0.003
70.	0.000	0.019	0.003
67.	0.000	0.019	0.003
63.	0.000	0.019	0.003
60.	0.000	0.019	0.003
57.	0.000	0.019	0.003
53.	0.000	0.018	0.003
50.	0.000	0.018	0.003
47.	0.000	0.018	0.003
43.	0.000	0.017	0.003
40.	0.000	0.017	0.003
37.	0.000	0.017	0.002
33.	0.000	0.016	0.002
30.	0.000	0.016	0.002
27.	0.000	0.015	0.002
23.	0.000	0.015	0.002
20.	0.000	0.015	0.002
17.	0.000	0.014	0.002
13.	0.000	0.014	0.002
10.	0.000	0.013	0.002
7.	0.000	0.014	0.002
3.	0.000	0.015	0.002

HBU92-0524

$$R = \frac{\text{MMW Variance}}{\text{Total Variance}} \times 100$$

Table 3.4-2 **Effect of Measurement Errors on the Target Position vs. Altitude Using Envelope Range Estimates. Impact Point 38.**

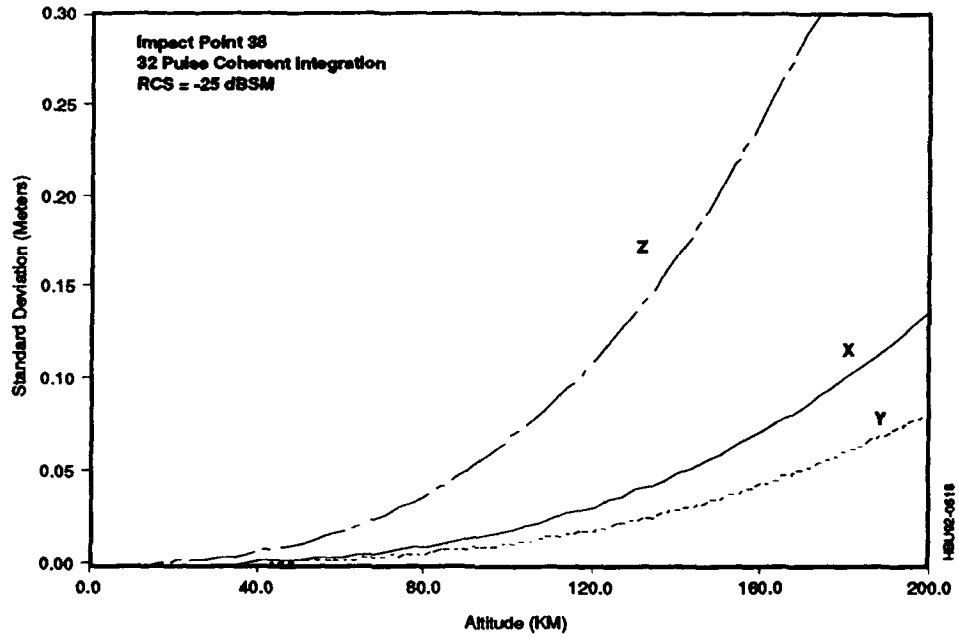

Figure 3.4-5 **Target Position Errors vs. Altitude Tradex Plus Two MMS Sensors. PDR Range**

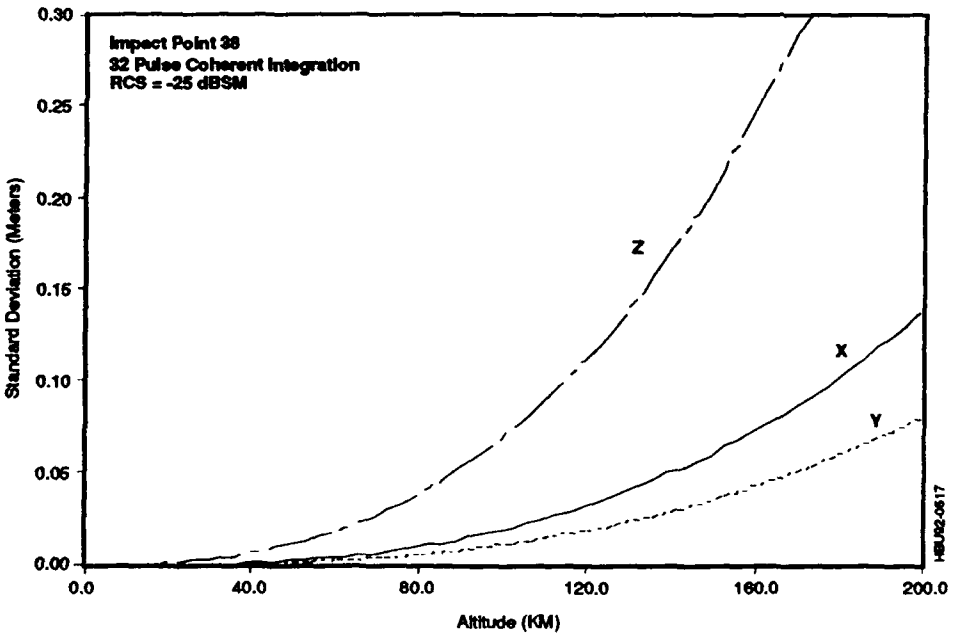

Figure 3.4-6 **Target Position Errors vs. Altitude MMW Plus Two MMS Sensors. PDR Range.**

Tradex

Alt. (KM)	R_x	R_y	R_z
120.	0.002	5.754	0.904
117.	0.002	5.732	0.900
113.	0.002	5.709	0.896
110.	0.002	5.685	0.892
107.	0.002	5.660	0.887
103.	0.002	5.633	0.883
100.	0.002	5.605	0.878
97.	0.003	5.576	0.873
93.	0.003	5.545	0.867
90.	0.003	5.512	0.862
87.	0.003	5.478	0.856
83.	0.003	5.441	0.850
80.	0.004	5.402	0.843
77.	0.004	5.361	0.836
73.	0.004	5.318	0.828
70.	0.005	5.271	0.820
67.	0.005	5.222	0.812
63.	0.005	5.169	0.803
60.	0.006	5.112	0.793
57.	0.006	5.052	0.783
53.	0.007	4.987	0.772
50.	0.008	4.917	0.761
47.	0.009	4.842	0.748
43.	0.010	4.760	0.734
40.	0.011	4.673	0.720
37.	0.013	4.579	0.704
33.	0.015	4.477	0.688
30.	0.017	4.368	0.670
27.	0.020	4.251	0.651
23.	0.024	4.128	0.631
20.	0.029	4.002	0.612
17.	0.036	3.879	0.593
13.	0.046	3.771	0.577
10.	0.062	3.705	0.569
7.	0.088	3.741	0.580
3.	0.137	4.022	0.636

$$R = \frac{\text{Tradex Variance}}{\text{Total Variance}} \times 100$$

MMW

Alt. (KM)	R_x	R_y	R_z
120.	0.000	0.087	0.013
117.	0.000	0.086	0.013
113.	0.000	0.086	0.013
110.	0.000	0.086	0.013
107.	0.000	0.085	0.013
103.	0.000	0.085	0.013
100.	0.000	0.084	0.013
97.	0.000	0.084	0.013
93.	0.000	0.083	0.012
90.	0.000	0.083	0.012
87.	0.000	0.082	0.012
83.	0.000	0.082	0.012
80.	0.000	0.081	0.012
77.	0.000	0.081	0.012
73.	0.000	0.080	0.012
70.	0.000	0.079	0.012
67.	0.000	0.078	0.012
63.	0.000	0.077	0.012
60.	0.000	0.077	0.011
57.	0.000	0.076	0.011
53.	0.000	0.075	0.011
50.	0.000	0.073	0.011
47.	0.000	0.072	0.011
43.	0.000	0.071	0.011
40.	0.000	0.070	0.010
37.	0.000	0.068	0.010
33.	0.000	0.067	0.010
30.	0.000	0.065	0.010
27.	0.000	0.063	0.009
23.	0.000	0.061	0.009
20.	0.000	0.059	0.009
17.	0.001	0.057	0.008
13.	0.001	0.056	0.008
10.	0.001	0.055	0.008
7.	0.001	0.055	0.008
3.	0.002	0.060	0.009

$$R = \frac{\text{MMW Variance}}{\text{Total Variance}} \times 100$$

HBU92-0525

Table 3.4-2 Effect of Measurement Errors on the Target Position vs. Altitude Using Phase Derived Range Estimates. Impact Point 38.

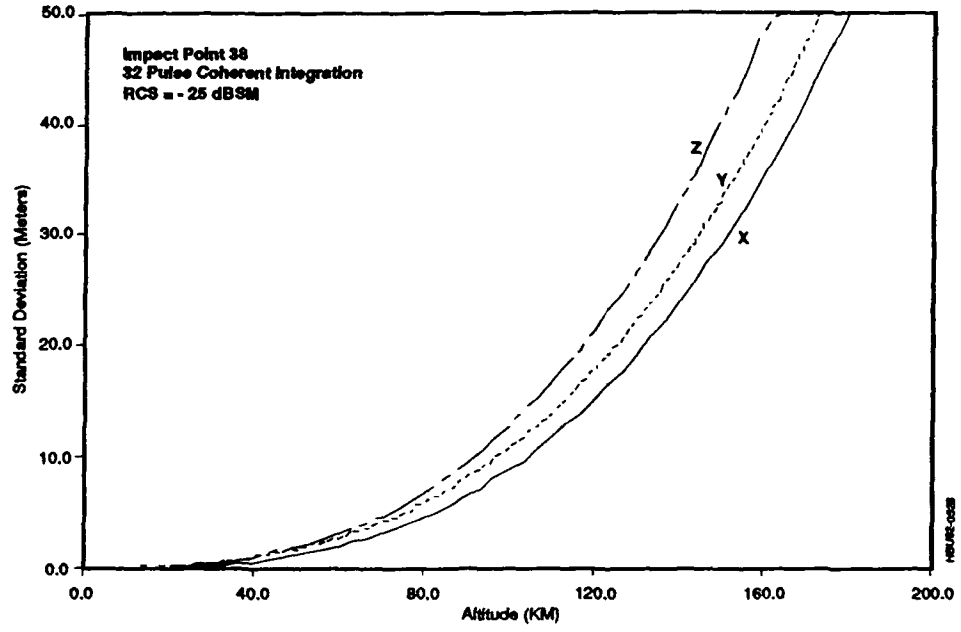

Figure 3.4-7 Target Position Errors vs. Altitude, Tradex Radar. Measurements: Az, El, Envelope Range

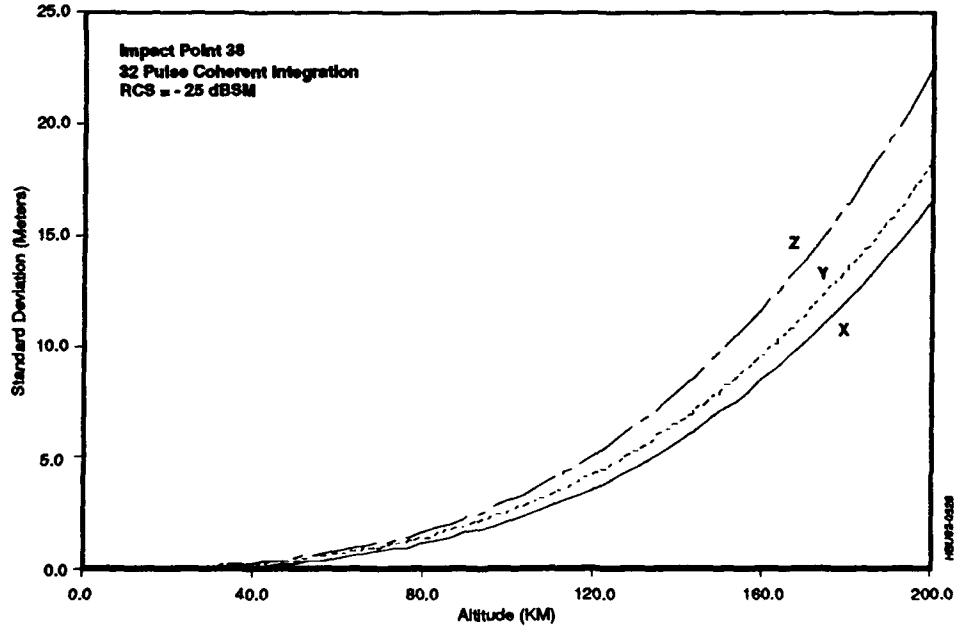

Figure 3.4-8 Target Position Errors vs. Altitude MMW Radar. Measurements: Az, El, Envelope Range.

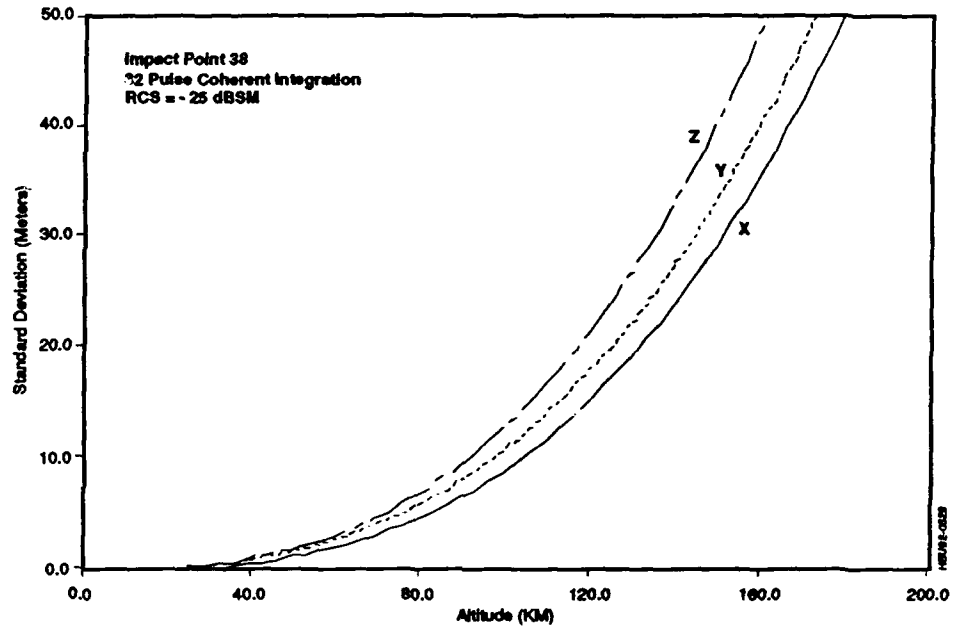

Figure 3.4-9 **Target Position Errors vs. Altitude, Tradex Radar. Measurements: Az, El, PDR Range.**

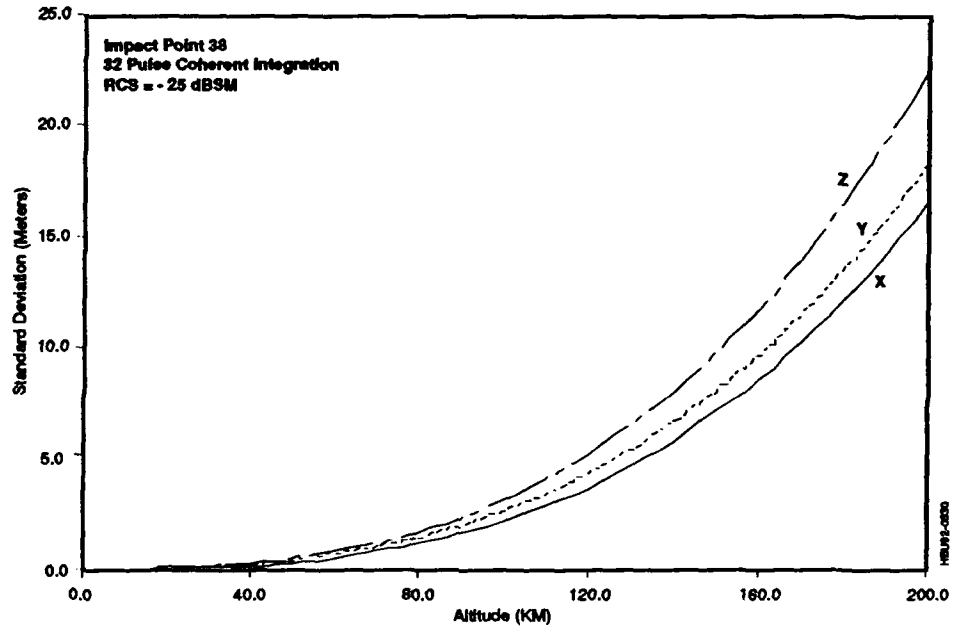

Figure 3.4-10 **Target Position Errors vs. Altitude, MMW Radar. Measurements: Az, El, PDR Range.**

3.5 Conclusion

The inclusion of the MMW sensor into the TRADEX-MMS system does not appear to significantly increase the accuracy of the target position errors, both for envelope and phase derived range measurements. The reason for this is that the two MMS sensors contribute to the majority of the position errors.

References

1. XonTech Report, 16 August 1984, XonTech Letter #6059 (SECRET), to Lester Kodama, Kentron HDRF, 233 Keawe Street, Honolulu, Hawaii 96813 (distribution included BMDSC-RO (Henry Cummings), BMDSCOM-RD, (John Weimer), and MIT/Lincoln Laboratory (Ray Holland). (This report indicated that the RMS phase jitter produced by the FPQ-19 on mission HAVE JEEP VI, Flight 2 premission sphere tracks was 8.3 degrees rms.)

2. Technical Manual for Radar Set AN/FPQ-19 (Modified from AN/TPQ/18 at KMR), Volume 1, System/Subsystem Descriptions, 1 July 1984.

3. Design of the Multistatic Measurement System, MIT/Lincoln Laboratory, Project Report RMP-169, October 1979.

4. Tristatic Tracking Filter Used by the Multistatic Measurement System, M.L. Smith, MIT/Lincoln Laboratory, Technical Report 699, September 1984.

5. TRADEX Data Users Manual, MIT/Lincoln Laboratory, Lincoln Manual 112 Rev. 2, December 1981.

6. ALCOR Data Users and Radar Operators Manual Ka and W bands, MIT/Lincoln Laboratory, Lincoln Manual 134, August 1983.

7. KMR Range Instrumentation and Support Facilities Manual, U.S. Army Kwajalein Atoll, January 1992.

8. Optimal Mismatched Filter Design for Radar Ranging, Detection and Resolution, R.J. McAulay, J.R. Johnson, MIT/Lincoln Laboratory,
Technical Note 1970-12, April 1970.